Use of Geogrids in Flexible Pavement Reinforcement
استخدام الشبكيات فى تقوية الرصف الاسفلتى

[1]Eman M. Ibrahim, [2]Sherif M. El-Badawy, [3]Mourad H. Z. Ibrahim

[1]Graduate Student, Public Works Engineering Department, Faculty of Engineering, Mansoura University, Mansoura 35516, Egypt, email: engemanmagdy@yahoo.com

[2]Associate Professor, Public Works Engineering Department, Faculty of Engineering, Mansoura University, Mansoura 35516, Egypt, phone: +201000183519, email: sbadawy@mans.edu.g

[3]Associate Professor, Public Works Engineering Department, Faculty of Engineering, Mansoura University, Mansoura 35516, Egypt, email: mouradhenry@yahoo.com

الملخص

استخدام الشبكيات فى تسليح قطاع الرصف الاسفلتى له تأثير ملحوظ علي أداء الرصف. لذا يهدف هذا البحث الي تحديد المكان الأنسب للتسليح في طبقة الأساس لتقليل اجهاد الكلال وبالتالي زيادة عمر الرصف، فى هذه الدراسه تم عمل اختبارات معمليه على قطاع أسفلت تم تنفيذه في المعمل يتكون من 5 سم طبقة أسفلت سطحية، 15 سم طبقة اساس من سن 6، و30 سم تربة طينية كطبقة تأسيس، حيث تم تسليح القطاع بطبقة من الشبكيات (RE540) وضعت علي ارتفاعات مختلفة بطبقة الأساس وتم قياس قيم الانفعال الناتج من التأثير علي القطاع بحمل استاتيكي متزايد عن طريق قرص التحميل أعلي ومنتصف وأسفل طبقة الأساس ، وتم مقارنة النتائج بقطاع رصف له نفس الخواص ولكن بدون تسليح. وقد بينت نتائج هذه الدراسة أن تسليح طبقة الأساس بصفة عامة يؤثر بشكل ايجابي علي قيم اجهاد الشد المقاسة وأن أنسب مكان للتسليح لرصف افضل أداء من حيث الكلال هو أعلي طبقة الأساس (تحت الأسفلت مباشرة) ثم علي ارتفاع 33% الي 50% بطبقة الأساس مقاسة من أسفل الطبقة.

Abstract

Effectiveness of geogrids as a reinforcement of the cross section of flexible pavement system was investigated. The study involved conducting of routine as well as advanced laboratory testing for comprehensive material characterization. It also included testing five large-scale pavement sections in the laboratory. These sections consists of a 5 cm asphalt layer (AC), 15 cm granular base layer, and a 30 cm clay subgrade. Five pavement sections were tested. The large-scale pavement sections were instrumented with strain gauges at different depth within the base layer. The base layer was reinforced with a single layer of RE540 uniaxial Tensar geogrid placed at four different positions within the base layer, one position at a time. These positions were 1) at the interface between the base and subgrade (B0), 2) 5 cm from the bottom of the base layer (B1/3h), 3) the middle of the base layer height (B1/2h), 4) and finally at the interface between the AC and base (Bh). These pavement sections were loaded with a static plate loading equipment until failure and the results were compared with the control section (CS) which had no reinforcement. Results from this study showed that geogrid can be used to improve the performance of flexible pavement systems. The position of the geogrid in the pavement system affects the performance significantly. The optimum position of the geogrid reinforcement to improve the pavement fatigue life was found to be directly underneath the AC layer then within 33 to 50% of the granular base layer height measured from the bottom of the base layer.

Keywords

Geogrid; Reinforcement; Resilient Modulus; Tensile strain; Large-scale laboratory test.

Received: 14 January, 2015 – Revised: 8 February, 2015 - Accepted: 8 February, 2015

Introduction

The majority of roads built in Egypt as well as many other countries in the world are flexible pavements. At some point of time this type of pavement may suffer from different distress types such as rutting and fatigue cracking. Thus, various materials used in the reinforcement of pavement materials and subgrade soils in order to accommodate the different distresses. They can vary greatly, either in form (strips, sheets, grids, bars, or fibers), texture (rough or smooth), and relative stiffness (high such as steel or relatively low such as polymeric fabrics), (Donald and Ohashi, 1983). Geosynthetics are a group of polymeric materials which are applied more and more in engineering projects, such as road and airport construction (Holtz, Christopher et al 1997). This research focuses on the use of the geogrids in pavement reinforcement. The main objective of the current paper is to find out the optimum position of geogrid in flexible pavement systems for the optimum performance.

Literature review

Kamel (2004) performed a laboratory program and finite element computer analysis to study the strength characteristics of both reinforced and unreinforced subgrade soils, Subbase, and base and to investigate their behavior under cyclic loadings. In the laboratory tests, Kamel used (CBR), unconfined compression, and triaxial compression tests to determine the optimum position of the grid by using two types of geogrids and three types of soils. The researcher placed the geogrid in a single layer at different positions of 20%, 40%, 60% and 80% of specimen height from the top surface. The reinforcement was placed in the base, subbase and subgrade layers. Kamel also used the ANSYS program to model the behavior of the reinforced pavement structure. The results indicated that the maximum effect of reinforcement was obtained when the geogrid was placed at 72-76% of the specimen height from top surface. The (CBR) of soil increased by 50-100% depending upon the type of soil and stiffness of the geogrid. The resilient strain of unreinforced soils decreased by 35% for all types of soils.

Penman and Cavanaugh (2007) used a geogrid within the unbound aggregate component of a flexible pavement to reduce rutting at the surface and fatigue cracking of the asphalt.

Virgile et al. (2009) evaluated the flexural behavior of bi-layer bituminous system reinforced with polyester and glass fiber geogrids through laboratory experiments. The results showed that the reinforced system improved the resistance to repeated cyclic loading from 66% to 100 %. It also delayed the inversion from decreasing to increasing rate of the permanent deformation evolution curve.

Moayedi et al. (2009) investigated the effect of geogrid reinforcement location in paved roads using axisymmetric pavement response model developed through the finite element program PLAXIS. Bituminous concrete layer and geogrid were modeled as a linear elastic isotropic material while the Mohr-Coulomb material model was used to simulate granular layers. Pavement responses were determined under static loading condition. The results reported that the geosynthetic reinforcement placed at the bottom of the bituminous concrete layer led to the highest reduction in vertical pavement deflection.

Zornberg and Gupta (2009) used falling weight Deflectometer (FWD) to evaluate the geogrid reinforced pavements constructed over expansive clays. The results showed that the geosynthetic reinforcements could be used to effectively minimize the development of longitudinal cracks.

Cartney et al. (2010) used field cyclic plate load (CPL) with geosynthetic reinforced sections. The tangent stiffness obtained from the third reloading cycle for

the pavement sections ranged from 495 to 905 kPa/mm during the winter (dry season), and 452 to 725 kPa/mm during the late spring (wet season).

Jersey et al. (2012) evaluated the performance benefits of a triaxial geogrid product in thin flexible pavements by comparing between reinforced and unreinforced cross sections. The results showed that the geogrid-reinforced pavement improved the resistance to rutting compared to the unreinforced control test.

Singh and Gill (2012) conducted CBR tests on selected soils, unreinforced and reinforced with geogrid. The geogrid was placed in a single layer at different positions: 20%, 40%, 60% and 80% of the specimen height from the top surface. A total of five samples of unreinforced and reinforced types were tested after soaking in water for four days. The results showed an increase in the CBR value from 2.9% without geogrid to 9.4% with geogrid reinforcement. The highest CBR value was achieved in subgrade when the geogrid was placed at 20% depth from the top of the specimen.

Al-Azzawi (2012) also used the ANSYS finite element program to find the optimum position of geogrid and the gained improvement in the behavior. The results showed that the geogrid reduced the vertical deflection and stresses developed in the model. The optimum position of geogrid was found to be at the interface between the base and Subbase layers.

Investigated Materials

In this research four different materials were investigated. These materials are a clay subgrade material typical in the delta region, a granular base material typically used in road construction in Egypt, wearing hot mix asphalt (HMA) layer, and finally the RE 540 Uniaxial High density Polyethylene Tensar geogrid. The subgrade soil was obtained from the south delta region (Zefta countryside). The granular base material was obtained from El Suez-Ataqa Quarry. The properties of the selected materials were determined in the laboratory and are shown in the next section. For the investigated geogrid, its properties were gathered from the manufacturer. The dimensions and mechanical properties of the Tensar RE540 geogrid used in this study are shown in Figure 1 and Table 1.

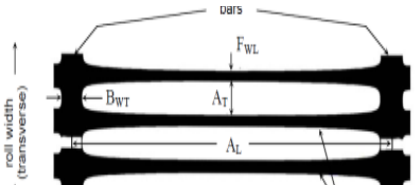

Figure 1. Tensar Geogrid Dimensions

Table 1. Properties of RE 540 Uniaxial Tensar Geogrid

Property	Grid-1(RE540)
Polymer	High density Polyethylene
Roll width (m)	1.3
Roll length(m)	50
Unit weight (kg/m^2)	0.45
Roll weight(kg)	31
Junction strength%	95
ULSpc or tcr for 25˚c (kN./m)	29.20
Short term tensile strength in longitudinal direction (kN./m)	64.5
Direct sliding coefficient αds	0.85
Pullout coefficient tαp	0.7

Experimental program

The experimental program consisted of laboratory routine and advanced material characterization as well as a laboratory large scale equipment test. All tests were conducted at the Highway and Airport Engineering Laboratory (H&AE-LAB) at Faculty of Engineering, Mansoura University.

Routine tests

In order to determine the routine properties of the unbound materials and subgrade soils, these materials were tested

in the laboratory. The test included, gradation, Atterberg limits, and modified proctor compaction for the base and subgrade soil layers. For the base material, bulk specific gravity, absorption, and disintegration in water were also conducted. A summary of the routine properties of the investigated unbound materials is given in Table 2. The grain size distribution of both the granular base material and subgrade soil is given in Figure 2.

Table 2. Routine Properties of the Investigated Unbound Materials

Physical Property	Subgrade Soil	Granular Base Layer
Soil Classification	A-7-6	A-1-b
P#200 (%)	91.1	5.3
Bulk Specific Gravity, G_{sb}	-----	2.468
Water Absorption (%)	-----	1.57
Disintegration (%)	-----	1.10
Liquid Limit (%)	59.1	23.0
Plasticity Index (%)	26.2	5.0
Max. Dry Density gm/cm^3	1.473	2.181
*OMC (%)	18.0	7.50

*OMC = optimum moisture content

The hot mix asphalt layer was designed using Marshall Method to comply with the 4-C gradation according to the Egyptian Specifications with an asphalt cement 60-70 penetration grade (ECP-2008). This is the typical grade commonly used in Egypt. The Job Mix Formula (JMF) of the mix is shown in Figure 3. The Marshall test results of the HMA layer is shown in Table 3.

Table 3. Marshall Properties

Property	4-C mix	Specifications
Penetration 0.01 mm	61.0	60-70
O.A.C	5.20	4 - 7.5
Stability(kg)	998	Min. 900
Flow mm	2.3	2 - 4
Density gm/cm^3	2.333	---------
A.V%	4.5	3 - 5
VMA%	15.7	Min.15
VFA%	71.2	---------
G_{mm}	2.423	AASHTO T 209

O.A.C = optimum asphalt content, A.V= air void, VMA= voids in mineral aggregate, VFA= voids filled with asphalt and G_{mm}= theoretical maximum specific gravity.

The static triaxial test was also conducted on the soil and granular base material using the Universal Testing Machine UTM-25 (manufactured by IPC) at the Highway and Airport Engineering Laboratory (H&AE-LAB) at Mansoura University. The UTM-25 is shown in Figure 4. This test was run in order to determine the shear strength parameters (Cohesion (c) and angle of internal friction (□)). Mohr coulomb failure envelopes for the subgrade and base layers along with the shear strength parameters are shown in Figures 5 and 6 respectively.

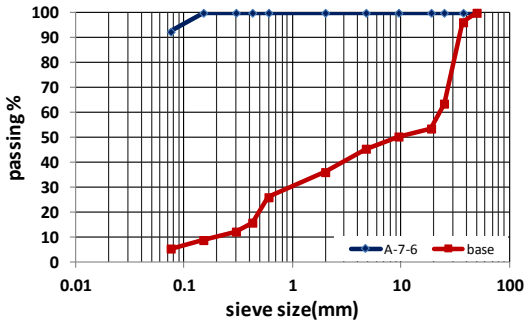

Figure 2. Gradiation of Subgrade and Base Material

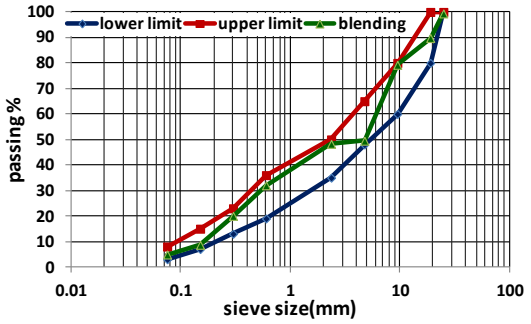

Figure 3. Job Mix Formula and the Specification Limits for the HMA Layer

Figure 4. The UTM-25 at H&AE LAB

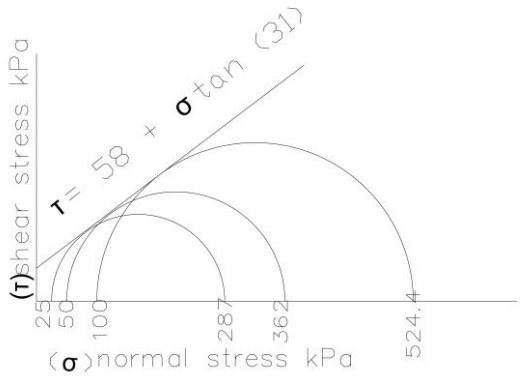

Figure 5. Mohr Coulomb for Subgrade Soil

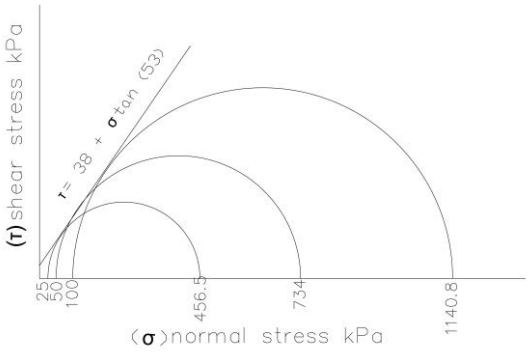

Figure 6. Mohr Coulomb for Granular Base

Advanced material characterization tests

The resilient modulus (Mr) of the unbound granular materials and subgrade soils is an advanced dynamic test used to assess the load carrying capacity of these materials. Thus, the UTM-25 was used to measure the Mr of the unbound materials investigated in this research according to AASHTO T-307 (2007). Three replicates of the subgrade as well as three other samples of the base material were compacted at the optimum moisture content and max dry density according to the modified proctor test. The dimensions of the clay samples were 10 cm diameter and 20 cm high while the granular base material samples were 15 cm diameter and 30 cm in height. Based on the testing results, nonlinear optimization technique was utilized to compute the K_1, K_2, and K_3 regression constants of the modified universal model shown in Equation (1) (ARA, 2004). The results are summarized in Table 4 for the subgrade soil and granular base material.

$$M_r = K_1 * p_a * (\theta / p_a)^{K2} ((\tau_{oct}/p_a)+1)^{K3} \quad (1)$$

Mr. =resilient modulus (psi)
□ = bulk stress =$\sigma_1+ \sigma_2+ \sigma_3$
σ_1 = major principle stress
σ_2 = intermediate principle stress
σ_3 = minor principle stress
τ_{oct} = octahedral shear stress=$1/3((\sigma_1-\sigma_2)^2+(\sigma_1-\sigma_3)^2+(\sigma_2-\sigma_3)^2)^{0.5}$
pa= atmospheric pressure 101kpa(14.7psi)
K_1, K_2, K_3 = regression constants

Table 4. K_1, K_2, and K_3 along with the Resilient Modulus Values of the Subgrade and Base Materials

	Subgrade soil	Granular base
K_1	0.503	1.2
K_2	- 0.297	0.65
K_3	2.403	0.059
σ_1(kPa)	41.4	110.4
σ_3(kPa)	13.8	55.2
Mr (Mpa)	76.14	205
R^2	0.2784	0.9738

R^2 = coefficient of determination

Laboratory large-scale test

The major laboratory test effort in this research was the large-scale equipment testing. Five flexible pavement sections with and without geogrid reinforcement were constructed, instrumented with dial and strain gauges and tested extensively in the laboratory. The pavement sections were built in a rectangular steel container. The dimensions of the steel container are: 1.0 m long, 0.35 m wide, and 0.55 m high. The front face of the container was made from a see-through acrylic material as

shown in Figure 7. A flexible pavement consisted of three layers: 5 cm AC, 15 cm granular base and 30 cm subgrade material was constructed inside the container. These thicknesses were selected to represent a typical pavement section for local roads in Egypt. The first large scale laboratory pavement section was the control section (CS). This section did not have any reinforcement. Then, four additional pavement sections were built, one at a time, inside the container and each section was reinforced with RE540 uniaxial Tensar geogrid at a specific location. The geogrid locations were selected to be within the base layer at different positions as follows: the interface between the base and subgrade (B0), at 1/3 of the height of the granular base (GB) layer from the bottom of the base layer (B1/3h), in the middle of the base layer height (B1/2h), and finally at the interface between the base layer and the AC layer (Bh). These cases are shown in Figure 8.

Figure 7. Laboratory Large Scale Equipment

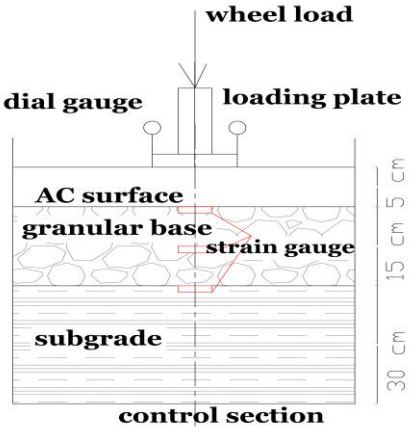

a) CS

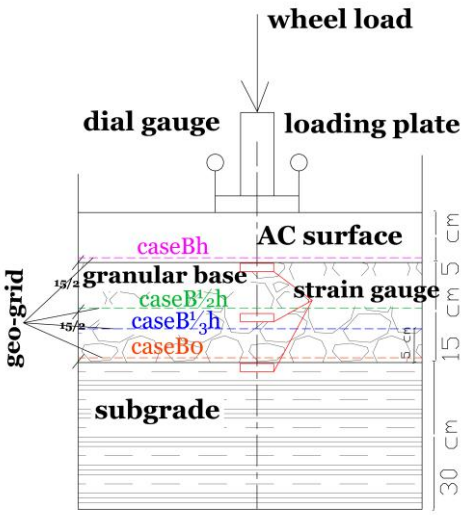

b) All cases(B0,B1/3h,B1/2h and Bh)

Figure 8. Cross Section of (a) Unreinforced and (b) Reinforced Pavement Sections

To place the materials inside the steel container, the subgrade was first placed in 2 layers and each layer was compacted to the maximum dry density and optimum moisture content according to modified Proctor given previously in Table 2. Each layer was compacted by a motorized rectangular steel plate 80*25*5 cm, and weighs about 20 kg. By trial and error it was found that 15 minutes of compaction using the motorized steel plate was enough to achieve the required density. The granular base layer was also compacted in two layers to achieve the required density, with each layer exposed to 10 minutes of compaction using the motorized steel plate. The sand cone test was conducted on each compacted layer in

order to check the achieved density for the base and subgrade layers as shown in Figure 9. Table 5 summarizes the relative density of the compacted layers for the 5 investigated pavement systems. The data in the table shows that the relative compaction was mostly within the specification limits.

Figure 9. Sand Cone on the Sugrade Layer

Finally, the surface AC layer of 5 cm was placed in a rectangular steel frame of 60*25*5 cm above the base layer and compacted for 3 minutes with mechanical steel plate and also compacted manually by the Marshall Compactor using only 5 blows. To check the compaction of the AC layer cores were taken after the test from the AC layer as shown in Figure 10 and density was determined. Table 6 shows the results of the cores densities. As compared to the required relative compaction of 97%, most of the results were generally fine.

Table 5. Achived Relative Compcation of the Large-Scale Base and Subgrade Layers

	Layer	Wc %	γ_{dry} gm/cm^3	Relative Compaction %
Case CS	Half depth of clay	19.0	1.441	98.2
	At surface of clay	19.5	1.452	98.7
	At surface of base	7.6	2.094	96.6
Case B0	Half depth of clay	18.6	1.451	98.8
	At surface of clay	18.2	1.442	98.5
	At surface of base	7.0	2.091	96.7
Case B1/3h	Half depth of clay	18.1	1.451	98.7
	At surface of clay	18.4	1.452	98.6
	At surface of base	6.9	2.092	96.5
Case B1/2h	Half depth of clay	18.1	1.443	97.8
	At surface of clay	19.5	1.432	97.8
	At surface of base	6.9	2.104	95.6
Case Bh	Half depth of clay	18.9	1.442	98.1
	At surface of clay	18.9	1.431	97.6
	At surface of base	7.1	2.071	95.4

Table 6. Densities and Relative Compcation of the AC Layer Determined From Cores

Case	Measured Density (gm/cm^3)	Relative Compaction %
CS	2.232	95.2
	2.271	97.1
B0	2.221	96.1
	2.212	95.5
B1/3h	2.312	98.2
	2.271	97.3
B1/2h	2.311	98.4
	2.321	98.1
Bh	2.210	97.2
	2.221	97.3

The hydraulic Jack of the plate load test was used to apply an incremental static load on a circular steel plate of 10 cm diameter placed on the asphalt surface. Regardless of the geogrid position, strains were monitored using strain gauges type PL-60-11-1L with gauge factor 2.07 ±1%, gauge resistance 120.3 ±0.5, transverse sensitivity 0.7%. The lab temperature

during the testing was between 18˚ and 23˚C. Strain gauges were placed at three constant positions in the large-scale laboratory system. The strain gauges were fixed at the interface between subgrade and base (sg_o), at the middle height of the base ($sg_{0.5h}$), and at the interface between base and AC layer (sg_h). For the strain gauge underneath the AC layer, the gauge was protected with carton and sealed with tapes to reduce the effect of the high temperature of the AC during the AC layer placement and compaction as shown in Figure 10. The strain gauges were connected to a strainometer model (P3 strain indicator and recorder) which automatically records the stain readings. At the same time the total surface deflection was monitored using dial gauges during the test.

Figure 10. Cores Taken From the AC Layer After Test

Figure 11. Stain Guges Under AC Layer

Experimental results and analysis

Figure12 shows the relationship between the applied stress and the measured tensile strain at the interface between the subgrade and the base layer (sg_o) for the five pavement systems. This figure shows that by reinforcing the base layer, a significant reduction in the measured tensile strain at the base/subgrade interface occurred compared to the control section. This is clear at the stresses anticipated in the field from truck traffic, which is approximately 828 KPa (120psi) at the surface of the AC layer. In addition, the lowest amount of strain occurred when the geogrid was placed within 33% to 50% of the base layer height as measured from the bottom of the base layer.

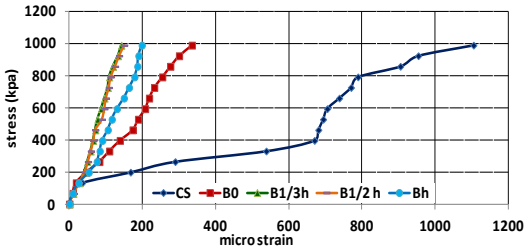

Figure 12. Stress versus Measured Strain at the Depth of the GB/SG Interface for all Cases

Moreover, Figures 13 and 14 show the relationship between the applied stress at the surface of the AC layer using the static plate load test and the measured tensile strain at the middle height of the base layer ($sg_{0.5h}$) and the interface between AC and granular base layer (sg_h), respectively. These figures again show a reduction in the measured strain at both locations when the base layer was reinforced with the geogrid compared to the control section. From Figure 13 it can be concluded that the reduction in the tensile strain was maximum at the middle of the base layer when the geogrid was placed at 1/3 of the base height as measured from the bottom of the base layer. Figure 14 shows that the lowest tensile strain at the bottom of the AC layer occurred when the geogrid was placed at the interface between the AC and granular base layer. It should be noted that the AC layer showed large deformation and it actually cracked under the loading plate for the control section only.

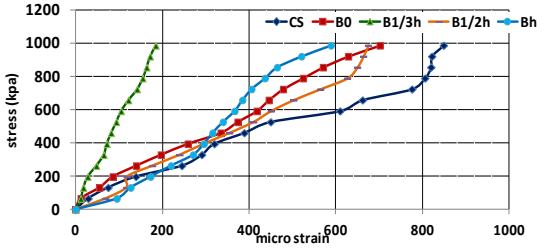

Figure 13. Stress versus Measured Strain at the Middle Depth of the Base Layer for all Cases

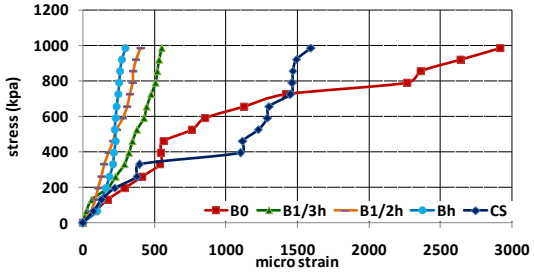

Figure 14. Stress versus Measured Strain at the Bottom of the AC Layer for all Cases

Figure 15 shows the cracks that occurred in the AC layer of the control section. In all other cases with geogrid reinforcement, under the same loading conditions, the AC layer was not fractured.

Figure 15. Cracks in AC Layer of the Control Section

Figure 16 shows a comparison of the strain values measured at a stress of 828 KPa which is equivalent to the stress anticipated in the field from typical truck wheel (ARA, 2004). The shown strains at the bottom of the AC layer indicate a significant reduction in the measured strain and hence longer pavement life with respect to fatigue cracking. The geogrids improved the pavement fatigue life through 1) increasing the bearing capacity of the granular layer underneath the AC layer, 2) the lateral restraint of the granular material, and 3) tensioned membrane effect (Giroud and Noiray 1981, Giroud et al. 1984, Perkins and Ismeik 1997, Holtz et al. 1998).

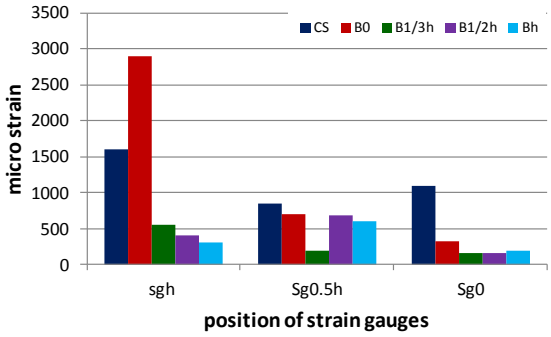

Figure 16. Comparison of the Strain Values Measured at a Stress of 828 kPa

The measured tensile strain values were also plotted against the depth for the five investigated cases and shown in Figure 17. The figure shows a decrease in the measured tensile strain values with depth for two out of the five cases which are B0 (geogrid at the interface between base and subgrade) and B1/3h (geogrid at 5 cm from the bottom of the base layer). The maximum reduction in the tensile strain occurred for case B0. However, one may notice that this case showed higher strains at the top of the granular base layer compared to the control section as well as the other investigated cases. One reason for this is stiffening effect occurred at the interface between the weakest layer (subgrade) and the moderate strength layer (granular base). This lead to a higher modular ratio and thus the AC showed higher strain compared to the underneath layer. This effect may led movement of the neutral axis within the AC layer and hence an increase in the tensile strain. The B1/3h showed a much better reduction in the tensile strains within the depth of the granular base layer compared to all other cases. The figure shows almost 3 times strain reduction at all depth compared to the control section. Finally this figure showed some increase in the measured tensile strain at the mid-depth of

the base layer compared to the other two depth (top and bottom of the base layer) for two cases which are Bh (geogrid at the AC/GB interface and B1/2h. This agreed with other literature studies (Perkins 2002). However, these two cases showed the highest reduction in the tensile strain at the bottom of the AC layer.

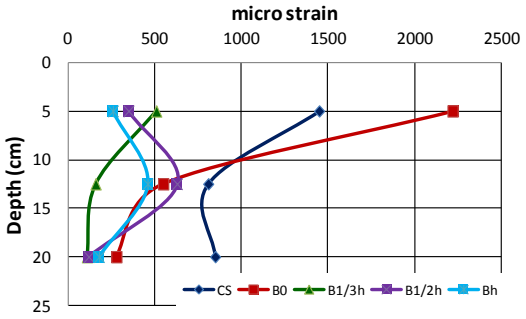

Figure 17. Relationship between Measured Tensile Strain and Depth for the Different Invistigated Cases

Summary and conclusions

This study investigated the effect of reinforcing the granular base layer using a Tensar RE540 uniaxial geogrid at different depth upon pavement fatigue life. A large-laboratory scale pavement section consisted of 5 cm AC layer, 15 cm granular base layer and 30 cm subgrade was built in steel container in the lab. The granular base layer was reinforced at four different depth 1) between the base and subgrade (B0), 2) 5 cm from the bottom of the base layer (B1/3h), 3) at the middle of the base layer height (B1/2h), 4) and finally at the interface between the AC and base (Bh). Load was applied using a static plate load test and strains were monitored at three positions: the interface between subgrade and base (sg_o), the middle height of the base ($sg_{0.5h}$), and the interface between base and AC layer (sg_h). Based on the results and analyses, the following conclusions were made:

- The reinforcement of the granular base layer with geogrid showed a significant reduction in the strain measured within the pavement system compared to pavement without reinforcement.
- The maximum reduction in the tensile strain at the bottom of the AC layer and hence the maximum fatigue life occurred when the geogrid was placed directly underneath the AC layer.
- The geogrids placed at 33% to 50% of the granular base height measured from the bottom of the base layer also yielded a great reduction in the measured tensile strain at the bottom of the AC layer as well as the top of the subgrade layer.
- When the geogrid was placed at the interface between GB/SG, there was some increase in the tensile strain at the bottom of the AC layer compared to the control section as well as the other investigated reinforcement cases. However the strain at the bottom of the GB layer was minimized.

Acknowledgments

The authors would like to acknowledge the support of TENSAR UK Internationals and their representative in Egypt Eng. Mohamed Higazy. The UTM-25 at Mansoura University H&AE LAB, which was utilized in this research was purchased as part of the HEI Labs Accreditation Project, 7th Cycle.

References

[1] AASTO T307-99, (2007), Standard Method of Test For Determining The Resilient Modulus of Soil and Aggregate Materials. American Associate of State Highway and Transportation Officials 444 North Capitol Street N.W., Suite 249 Washington D.C 20001.

[2] Adel A. Al-Azzawi (2012), Finite Element Analysis of Flexible Pavements Strengthen With Geogrid, ARPN Journal of Engineering and Applied Sciences, VOL. 7, NO. 10.

[3] ARA, INC., ERES Consultants Division (2004) "Guide For Mechanistic Empirical Design of

New and Rehabilitated Pavement Structures, NCHRP 1-37A Final Report, Transportation Research Board, National Research Council, Washington , D.C.

[4] Donald, H. Gary, and Harukazu Ohashi, (1983), Mechanics of Fiber Reinforcement in Sand, Journal of Geotechnical Engineering, ASCE, Vol .109(3), PP. 335-353.

[5] Giroud, J. P. and Noiray, L. (1981), Geotextiles - Reinforced Unpaved Roads. Journal of Geotechnical Engineering Division, American Society of Civil Engineers, Vol. 107, No GT9, pp. 1233-1254.

[6] Giroud, J. P., Ah-Line, C., and Bonaparte, R. (1984), Design of Unpaved Roads and Trafficked Areas with Geogrids. Polymer Grid Reinforcement, A Conference Sponsored by SERC and Netlon, Ltd., Thomas Telford, London, England, pp. 116-127.

[7] Holtz, R. D, Christopher, B. R. and Berg, R. R. (1998), Geosynthetic Design and Construction Guidelines. U.S. Department of Transportation, Federal Highway Administration, Washington, DC, FHWA-HI- 98-038, 460 p.

[8] Holtz, R. D., Christopher, B. R. and Berg, R.R., (1997) Geosynthetic Engineering, BiTech Publishers Ltd., Canada.

[9] J. G. Zornberg and R. Gupta (2009), Reinforcement of Pavements Over Expansive Clay Subgrades, 17th International Conference on Soil Mechanics and Geotechnical Engineering.

[10] Moayedi, H., Kazemian, S., Prasad, B. and Huat(2009), Effect of Geogrid Reinforcement Location in Paved Road Improvement, Journal of EJGE, Vol.14, pp.3313-3329.

[11] Moustafa Abd El Ghaffar, (2004). Development of Design Procedure For Reinforced Flexible Pavement, PhD Dissertation, Department of Civil Engineering Indian Institute of Technology Roorkee 247667, India.

[12] Pardeep Singh and K. S. Gill (2012), CBR Improvement of Clayey Soil with Geogrid Reinforcement, International Journal of Emerging Technology and Advanced Engineering, ISSN 2250-2459, Volume 2, Issue 6.

[13] Penmam, J. and Cavanaugh, J., (2007), Extending Flexible Pavement Life Using Geogrid, TENSAR International Corporation.

[14] Perkins, S. W. (1999), Mechanical Response pavements. Geosynthetics International, Vol. 6, No. 5, pp. 347-382.

[15] Perkins, S. W. (2002),Evaluation of Geosynthetic Reinforced Flexible Pavement Systems Using Two Pavement Test Facilities, FHWA/MT 02-008/20040.

[16] Perkins, S. W. and Ismeik, M. (1997a), ASynthesis and Evaluation of Geosynthetic-Reinforced Base Course Layers in Flexible Pavements: Part I Experimental Work. Geosynthetics International, Vol. 4, No. 6, pp. 549-604.

[17] Perkins, S. W. and Ismeik, M. (1997b), A Synthesis and Evaluation of Geosynthetic-Reinforced Base Course Layers in Flexible Pavements: Part II Analytical Work. Geosynthetics International, Vol. 4, No. 6, pp. 605-621.

[18] Sarah R. Jersey, Tingle J., and Gregory J. Norwood (2012), Full scale Evaluation of Geogrid Reinforced Thin Flexible Pavement, TRB Annual Meeting.

[19] TENSAR International Limited, Units 2-4 Cunningham Court,Shadsworth Business Park, Blackburn, BB1 2QX, United Kingdom Reinforced fill product Certificate No. RF 2/2013 TENSAR RE500 Geogrids.

[20] Virgili A., Canestrari F., Grilli A., Santagata F. (2009). Repeated Load Test on Bituminous Systems Reinforced by Geosynthetics. Geotextiles and Geomembranes. 27 (3): 187195.

[21] Zornberg J., Bouazza A., McCartney J. (2010). Geosynthetic Capillary Barriers: Current State of Knowledge. Geosyn. Int., 17(5): 273-300.